Journal of Alloys and Compounds 509 (2011) 4018–4024

Contents lists available at ScienceDirect

Journal of Alloys and Compounds

journal homepage: www.elsevier.com/locate/jallcom

Crystallization properties of RE-doped (RE = Eu, Er, Tm) Zn_2TiO_4 prepared by the sol–gel method

Jan Mrázek[a,*], Lubomir Spanhel[b], Martin Surýnek[b], Michel Potel[b], Vlastimil Matějec[a]

[a] Institute of Photonics and Electronics AS CR, v.v.i., Chaberská 57, 18251 Prague 8, Czech Republic
[b] Université de Rennes 1, Sciences Chimiques de Rennes, UMR-CNRS 6226, Campus de Beaulieu, CS74205, F-35042 Rennes Cedex, France

ARTICLE INFO

Article history:
Received 8 November 2010
Received in revised form
30 December 2010
Accepted 3 January 2011
Available online 5 January 2011

Keywords:
Zinc titanate
Rare earth element
Sol–gel processes
Nanostructured materials
Crystal growth

ABSTRACT

Samples of pure and rare earth (RE)-doped nanocrystalline Zn_2TiO_4 (RE = Eu, Er, Tm) have successfully been prepared by the single batch sol–gel method in a form of powders. The powders were annealed up to 1200 °C and analyzed by DTA and XRD methods. Sizes of formed nanocrystals were calculated from the Scherer equation and verified by the SEM analysis. Activation energies of crystallization were calculated using the Kissinger, Ozawa and Augis–Bennett approximations and reaction mechanisms were proposed evaluating the Avrami exponents from the Johnson–Mehl–Avrami equation. It has been found that RE elements particularly substitute zinc ions in the crystal lattice and are fully soluble up to 0.5 at.% related to the some of cations. Furthermore, the results have shown that the presence of RE elements blocks the crystallite growth and supports the nucleation process leading to the formation of smaller and more uniform nanocrystals compared to the undoped Zn_2TiO_4.

1. Introduction

Zinc titanate – Zn_2TiO_4 has attracted great attention in the field of material sciences within last decades. Its inverse spinel structure and high thermal stability [1] have made it attractive as a catalyst for desulphurization [2] and dehydrogenation [3] processes and as a pigment [4]. Recently, it has been introduced as the fundamental constituent of low-temperature sintered ceramics for microwave dielectrics [5,6]. Its optical properties have also been intensively investigated [7,8]. To improve its photoluminescence properties vanadium, chromium and tin ions were introduced as dopants inside the zinc titanate matrix [9] which resulted into an increased emission due to the distortion of the periodic structure. Moreover, zinc titanate has successfully been used as a host matrix for rare earth elements such as Eu [10], similarly as yttrium aluminum garnets (YAG) [11] or zinc aluminate matrices [12]. However, it has been shown that for successful improvement of physico-chemical properties of this material its crystalline structure should be precisely tailored [5,6]. Various methods have been employed for the Zn_2TiO_4 synthesis including the solid-state reaction [1], magnetron reactive sputtering [7], hydrothermal process [6] and sol–gel method [9,10]. From these methods the sol–gel route and hydrothermal process offer the best control over the formation of crystalline materials.

In this contribution we have employed already described sol–gel route [10] for the preparation of zinc titanate powders either undoped or doped with Eu and newly with Er and Tm which are stable at high temperatures and exhibit tailored crystalline properties. The preparation of these powders creates basis for the investigation of crystallization processes in these materials as well as the solubility of RE in Zn_2TiO_4 matrices and is aimed in preparing nanocrystalline materials without side-formed RE pyrochlorates. In this paper typical properties are presented for undoped and Eu-doped Zn_2TiO_4 and general results are subsequently extended for Er- and Tm-doped samples.

2. Experimental

2.1. Preparation

Powders were prepared by the sol–gel method. All chemicals were used without further purification. Typically 6.56 g of titanium(IV)butoxide (Fluka, Purum) was dissolved under regular stirring in 250 ml of absolute ethanol (Sigma–Aldrich, Spectranal grade) then 8.46 g of zinc acetate dihydrate (Fluka, ACS reagent) was added into solution and stirred under ambient temperature forming transparent solution. The mixture was refluxed at 86 °C for 24 h and then cooled down to the laboratory temperature. Optionally, 0.5–8 at.% of $Eu(NO_3)_3{\cdot}5H_2O$, $Er(NO_3)_3{\cdot}5H_2O$ or $Tm(NO_3)_3{\cdot}5H_2O$ (Aldrich, 99.9%) (with respect to the overall Zn and Ti content) was dissolved in the formed heterosols in an ultrasonic bath and the sols were stirred at the ambient temperature for 6 h. The prepared sols were purified by filtration through 0.2 μm PTFE membrane and the filtrates were evaporated on a rotary evaporator under a reduced pressure (30–40 mbar) and temperatures rising from 40 to

* Corresponding author. Tel.: +420 266 773 558; fax: +420 284 680 222.
E-mail address: mrazek@ufe.cz (J. Mrázek).

0925-8388/$ – see front matter © 2011 Elsevier B.V. All rights reserved.
doi:10.1016/j.jallcom.2011.01.009

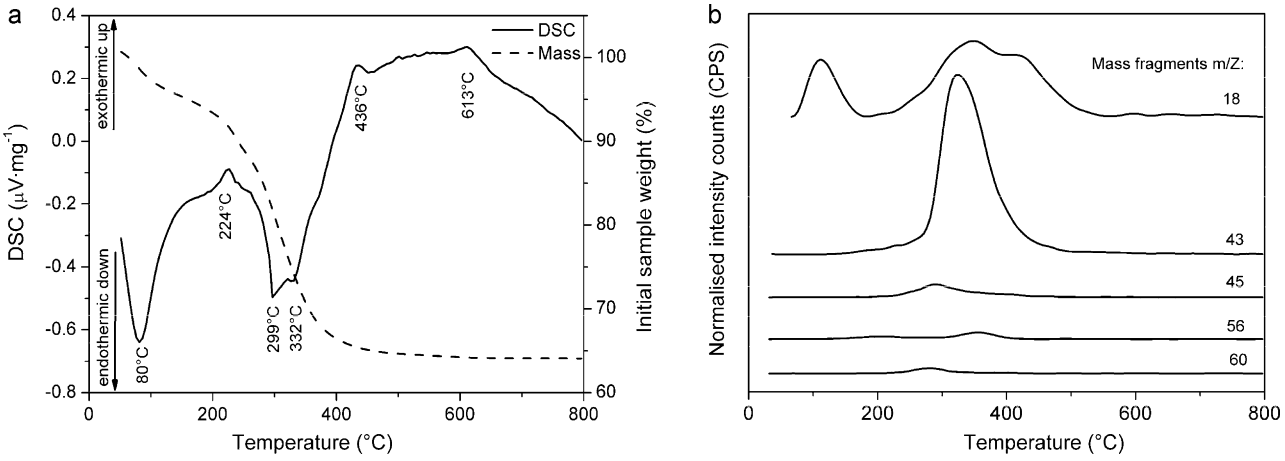

Fig. 1. (a) DSC–TG curves of Zn_2TiO_4 sample containing 1 at.% Eu (b) corresponding MS spectra for selected fragments.

70 °C. The resulting powders were directly used in measurements or in air atmosphere heated with a heating rate 10 °C min^{-1} to temperatures in a range from 200 °C to 1000 °C where they were kept for 1 h.

2.2. Characterization

The burnout and crystallization properties of the prepared powders were analyzed by thermal analysis (TA), thermogravimetry (TG) and differential scanning calorimetry (DSC) followed by mass spectroscopy (MS) and infrared spectroscopy (FT-IR). The TA, TG, DSC and MS measurements were carried on Netzsch STA449C multifunctional apparatus. To determine the liberation of organic compounds during the heat treatment some powder samples were analyzed by DSC method coupled with MS at a heating rate of 10 °C min^{-1} up to 800 °C under a nitrogen flow of 50 ml min^{-1}. Crystallization properties of the prepared powders were determined by the DSC analysis of the powder samples pre-treated at temperatures to 300 °C in air in order to evaporate volatile fractions of organic compounds. These samples were further treated at different heating rates from 15 to 30 °C min^{-1} under an oxygen flow of 50 ml min^{-1}. In all these experiments approximately 10 mg of powder samples was used.

The FT-IR spectra of the prepared powders were recorded with a Bruker Vector 22 spectrometer. At these measurements, approximately 4 mg of the powder was mixed with 200 mg of KBr (Sigma–Aldrich, 98% FT-IR grade) finely pulverized in a mortar and pressed into a pellet. The blank sample made of pure KBr was used as the reference.

The XRD structural analysis of the prepared powders was performed on a Bruker D8 diffractometer with the Bragg–Brentano geometry operating with the Cu-Kα radiation (λ = 1.54056 Å, operating voltage 40 kV, current 40 mA, integration time 200 ms). Recorded data were evaluated by the Origin8. Diffraction peaks were fitted by the Gaussian curves to calculate the full-width at half-maximum (FWHM) values. The instrumental broadening of the peaks was correlated to the diffraction (2 0 0)-plane peak of KCl (Sigma–Aldrich, ACS reagent). Crystallite and grain sizes D were calculated from the Scherrer equation – Eq. (1) [13]:

$$D = \frac{k \cdot \lambda}{\beta \cdot \cos\theta}, \quad (1)$$

where k is the structural factor equal to 0.89, λ is the X-ray wavelength equal to 0.15406 nm, β is the correlated FWHM value corresponding to the (3 1 1)-plane peak of Zn_2TiO_4 at the diffraction angle θ. Particular phases were identified by JCPDS data files number 25-1164, 36-1451, 23-1072, 18-0499 and 23-0590 for Zn_2TiO_4, ZnO, $Eu_2Ti_2O_7$, $Er_2Ti_2O_7$ and $Tm_2Ti_2O_7$, respectively.

SEM images of the sintered powder samples were taken with a Philips XL30 ESEM electron microscope. The overall chemical composition was verified by elemental analysis on a JEOL JSM 6400 electron microscope equipped with an Oxford instrument EDS analyzer. The chemical compositions of individual grains were measured on the powders heat-treated to 1200 °C for 24 h by a Cameca SX100 electron microprobe. A thin palladium layer was sputtered onto the samples prior to the analysis to prevent powder samples charging.

3. Results and discussion

3.1. Burn-out behavior

The thermal treatment of sol–gel based materials is complex process including the decomposition of organic compounds, various chemical reactions and crystallization processes. The thermogravimetric results (see Fig. 1a) indicate two main mass losses which can be linked with two endothermic peaks on the DSC curve. According to the MS results (see Fig. 1b) the first step bellow 130 °C can be attributed to the evaporation of water (m/z = 18) and volatile compounds such as residual ethanol. The second step in a temperature range from 224 to 430 °C can be related to the second broad endothermic peak and it is accompanied by liberation of water (m/z = 18) and organic ligands based on acetate fragments such as acetic acid (m/z = 43, 45, 60) and butylacetate (m/z = 43, 56). The decomposition of organics is followed by slow dehydratation and can be related to the third endothermic peak at 456 °C. Finally, the crystallization of Zn_2TiO_4 occurs at 613 °C. Despite the high concentration of Eu ions in the sample the crystallization peak corresponding to the formation of $Eu_2Ti_2O_7$ has not been observed.

The MS record was followed by the FT-IR measurements to verify the character of liberated organics and coordination modes of organic ligands toward central atoms (see Fig. 2). As expected the prepared powders contain large amount of organic materials. Absorption bands linked with CH_3– organic group can be found at 1026 and 1052 cm^{-1} representing CH_3 rock vibrations, at 1343 cm^{-1} and 1414 cm^{-1} representing $\delta_s(CH_3)$, $\delta_{as}(CH_3)$ [14], respectively. Bands at 522, 613 and 692 cm^{-1} can be attributed to γ(COO), π(COO) and α(COO), respectively [14,15]. Two broad bands centered around 1450 and 1571 cm^{-1} are attributed to stretching vibrations of carboxylic groups coordinated on metal ions [16]. From the difference between the position of bands corresponding to asymmetric (1565 and 1550–1590 cm^{-1} for Zn and Ti, respectively)

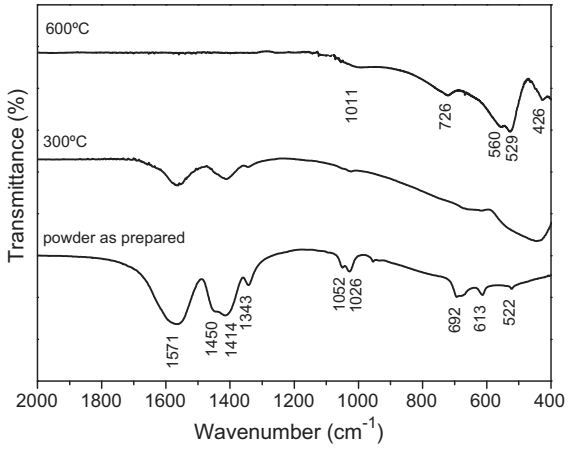

Fig. 2. FT-IR spectra of Zn_2TiO_4 powders heat-treated at different temperatures.

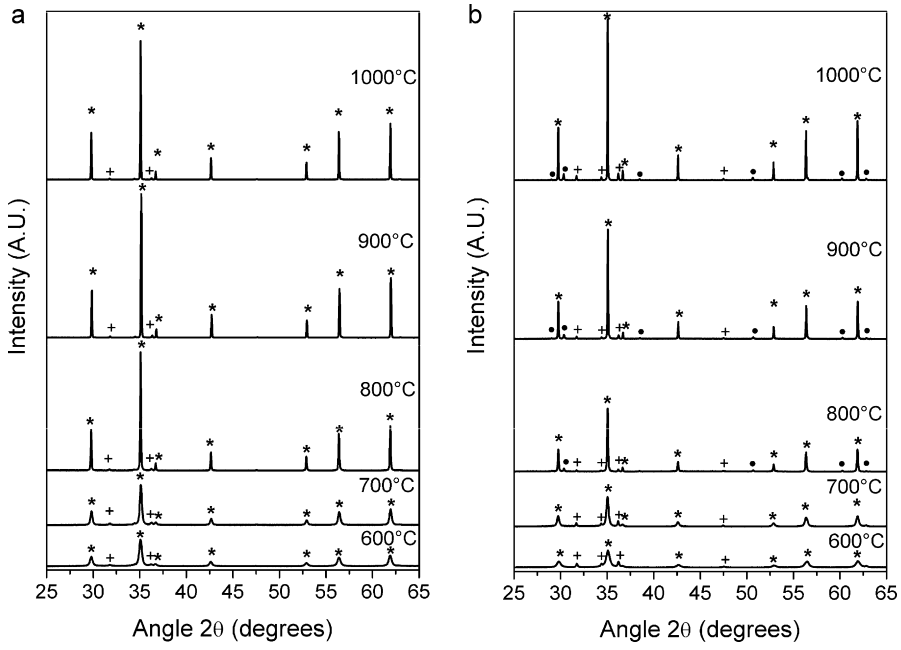

Fig. 3. XRD records of (a) undoped Zn_2TiO_4 and (b) Zn_2TiO_4 containing 1 at.% of Eu heat-treated at different temperatures. (*) Zn_2TiO_4, (+) ZnO and (•) $Eu_2Ti_2O_7$.

and symmetric (1450 and 1414 cm^{-1} for Zn and Ti, respectively) vibrations of COO^- groups we can estimate the presence of bridging bidentate ligands bonded to Ti and chelating bidentate ligands bonded to Zn ions [14,16]. The measured spectra show that by increasing the temperature, organic ligands are gradually burned out and corresponding absorption bands diminish which correlates with the DSC–TG measurements discussed above. Acetates coordinated to Zn ions are burn out at lower temperatures than ligands attached to Ti ions which can be drawn from the practically disappeared absorption band at 1450 cm^{-1} attributed to acetates bonded to Zn ions and from comparison with the absorption band of acetates bonded to Ti ions at 1414 cm^{-1} at 300 °C. Thus, at this temperature mainly bridging bidentate ligands bonded to Ti ions remain in the mixture. These measurements explain why the traces of ZnO can be formed prior to the crystallization of Zn_2TiO_4 due to the easier accessibility of zinc ions. Once the crystallization takes place and periodic structure of inverse spinel Zn_2TiO_4 is formed bellow 600 °C, new sharp absorption bands related to $[TiO]_6$ and $[ZnO]_4$ groups [9,17,18] appear in FT-IR spectra.

3.2. X-ray diffraction study

The overall XRD spectra for undoped Zn_2TiO_4 and for sample containing 1 at.% of Eu are shown in Fig. 3a and b, respectively. These spectra show that the crystallization of inverse spinel Zn_2TiO_4 starts at 560 °C and the introduction of Eu ions significantly blocks the crystallization process. Consequently, the size of formed crystallites calculated from the presented XRD spectra by using Eq. (1) progressively decreases with increasing Eu concentration as shown in Fig. 4a. By increasing the temperature, nanocrystals regularly grow and the calculated size increases too (see Fig. 4b). The results in Fig. 4b are in good agreement with the results of SEM measurements of the heat-treated powders shown in Fig. 5. On the basis of Fig. 5 one can conclude that the formed crystallites are well homogeneous without preferentially oriented shapes and the presence of Eu ions increases the uniformity of nanocrystals. Traces of ZnO which was formed prior to the crystallization of Zn_2TiO_4 were detected in the heat-treated powders and the amount of crystallized ZnO was constant independently of heat-treating temperature (see Fig. 3a). However, in the samples with intro-

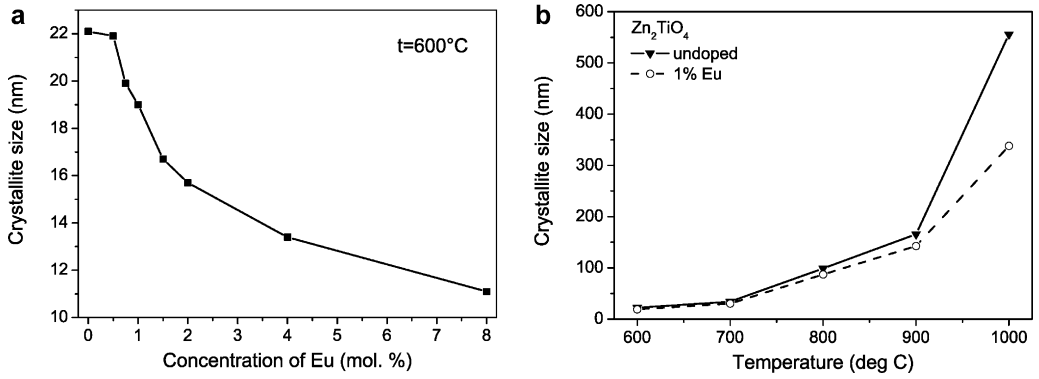

Fig. 4. The crystallite size of Zn_2TiO_4 as a function of (a) Eu concentration for samples heat-treated at 600 °C and (b) different heat-treating temperatures for undoped and Eu doped samples.

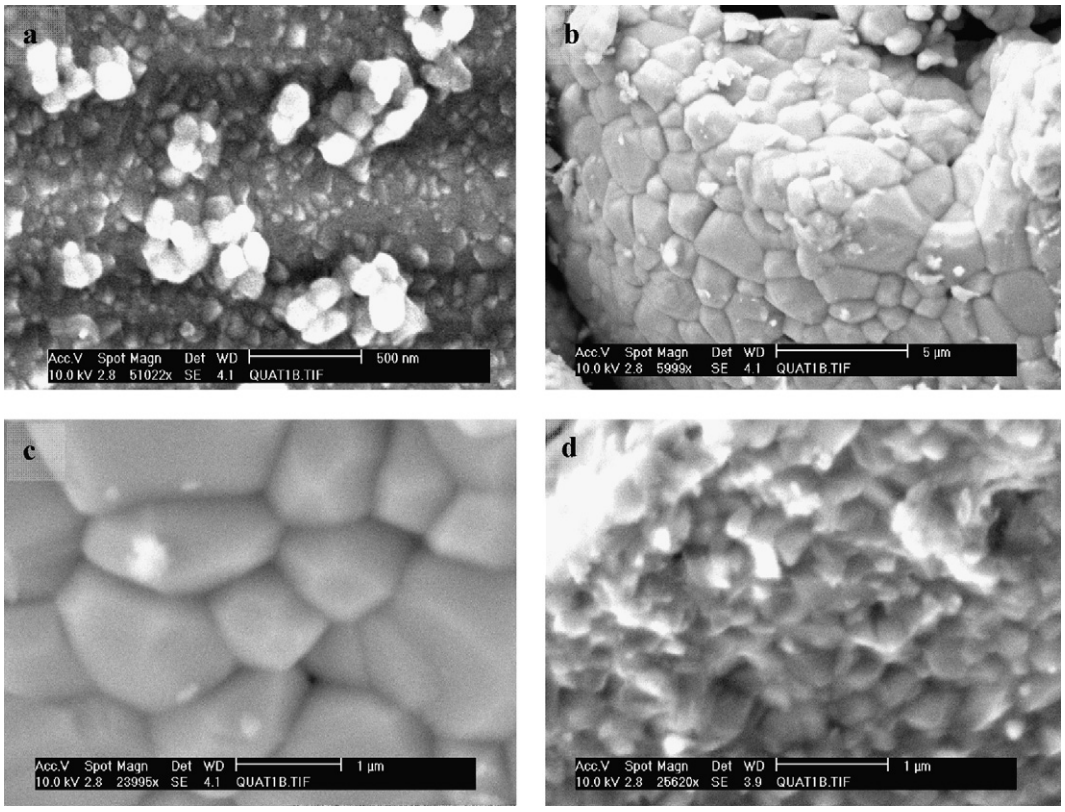

Fig. 5. SEM images of overall surface of undoped Zn_2TiO_4 heat-treated at (a) 600 °C and (b) 1000 °C and the zoom of (c) undoped Zn_2TiO_4 and (d) Zn_2TiO_4 containing 1 at.% of Eu both heat-treated at 1000 °C.

duced Eu ions a slightly higher ZnO concentration was observed (see Fig. 3b).

If the concentration of Eu in the sample exceeds its solubility limit a new crystalline phase of europium pyrochlorate – $Eu_2Ti_2O_7$ is formed as one can see from XRD spectra in Fig. 3b. To clarify crystallization processes, the volume fraction of a particular crystalline phase was evaluated from the measured XRD spectra by using Eq. (2) [19]:

$$\text{Volume\_fraction}\ (\%) = \frac{A_{\text{phase}}}{A_{\text{allpeaks}}} \cdot 100, \qquad (2)$$

where A_{phase} is the integral area of XRD peaks belonging to the evaluated phase and A_{allpeaks} is the integrated area of all XRD peaks of overall XRD record. The thermal evolution of the volume fraction of zinc titanate for different Eu concentrations can be seen in Fig. 6. The curves in Fig. 6 show that the volume fraction of undoped Zn_2TiO_4 is practically constant and close to 100% with

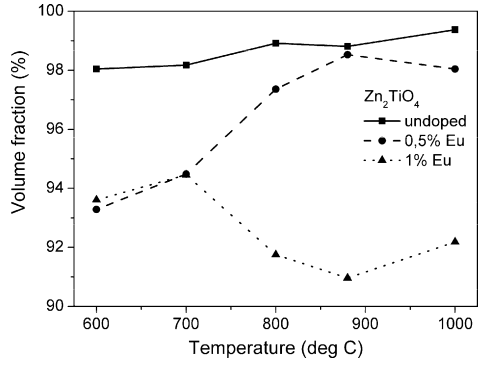

Fig. 6. Thermal evolution of the volume fraction of Zn_2TiO_4 for undoped and Eu-doped samples.

Table 1
Results of the local chemical analysis of particular grains of samples heat-treated at 1200 °C for 24 h.

Dopant	Zn (at.%)	Ti (at.%)	RE (at.%)
Undoped Zn_2TiO_4	65.95 ± 0.30	34.05 ± 0.36	–
Eu	59.86 ± 0.37	39.60 ± 0.42	0.54 ± 0.05
Tm	63.63 ± 0.37	35.82 ± 0.43	0.55 ± 0.05
Er	63.96 ± 0.34	35.60 ± 0.38	0.44 ± 0.06

respect to low concentrations of the residual ZnO. In samples containing Eu ions the growth of zinc titanate is blocked and samples contain ZnO formed after the burn-out of organic ligands. Consequently, the crystallinity of such samples at low temperatures is rather lowered comparing to the undoped sample. The crystallinity continuously increases with increasing the heat-treatment temperature. This result holds only for samples where the concentration of Eu does not exceed of about 0.5 at.%, which can be estimated as the solubility limit. If the concentration of Eu is higher than the limit (e.g. 1 at.%) the break corresponding to the crystallization of new phase $Eu_2Ti_2O_7$ appears on the curve.

Similar processes were observed with erbium and thulium ions forming corresponding pyrochlorates. To confirm the displacement of RE elements in the matrix and their solubility local microanalysis of individuals grains were carried out. Their results are summarized in Table 1. Although the overall elementary analysis employing the EDS method determined contents of 66.48 and 33.53 at.% of zinc and titanium, respectively, in all samples, the content of zinc in individual grains is slightly decreased particularly in samples containing rare earth elements. Such concentration difference and crystallization behavior can be explained on the basis of a mechanism that RE elements particularly substitute zinc in the matrix and that concentrations higher that the solubility limit of RE lead to the decomposition of doped zinc titanate into zinc oxide and cor-

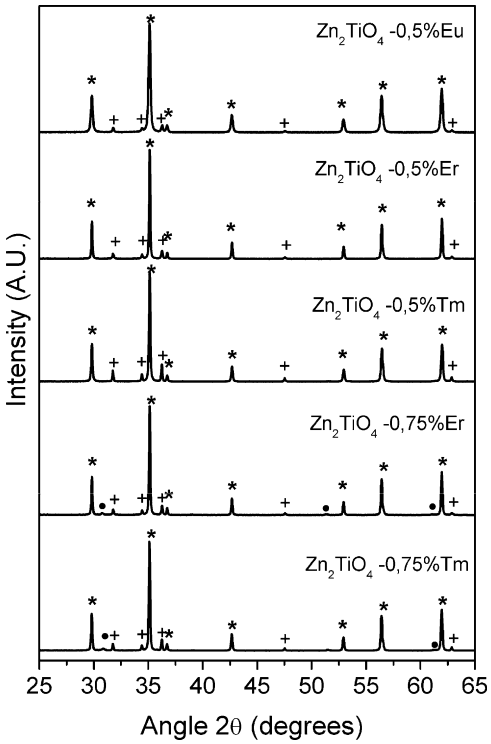

Fig. 7. XRD records of samples Zn_2TiO_4 containing 0.5 at.% and 0.75 at.% of Eu, Er and Tm, respectively heat-treated at 800 °C. (*) Zn_2TiO_4, (+) ZnO and (•) $RE_2Ti_2O_7$, RE = Eu, Er, Tm.

responding RE pyrochlorate. In order to test this mechanism and validate the quantitative chemical analysis, zinc titanates doped by 0.50 and 0.75 at.% of RE elements were prepared. Their XRD spectra are presented in Fig. 7 and show that an increase of Er and Tm concentrations to 0.75 at.% is related to the formation of RE pyrochlorates.

3.3. DTA study

The activation energy of crystallite growth can be calculated from Eq. (3) [20]:

$$\log(D) = \frac{-Q}{2.303 \cdot R} \cdot \frac{1}{T} + A, \tag{3}$$

where D mean the average crystallite size, Q is the activation energy of the crystallite growth, R is the ideal gas constant, and A is the integration constant. The values of $-Q/(2.303 \cdot R)$ are accessible by fitting the plot of $\log(D)$ versus the reciprocal absolute temperature $(1/T)$ (see Fig. 8). The determined activation energies of

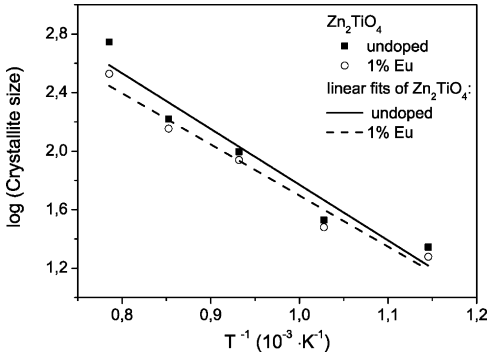

Fig. 8. Thermal evolution of the crystallite size used for the determination of activation energy of crystallite growth for undoped and Eu-doped Zn_2TiO_4.

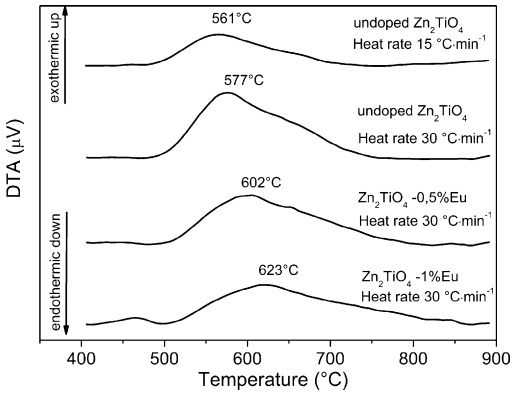

Fig. 9. DTA analysis of different Zn_2TiO_4 powders pre-treated in air at 300 °C.

crystallite growth were 72.8 ± 10.5 and 66.9 ± 7.1 kJ mol^{-1} for the undoped sample and the sample containing 1 at.% Eu ions, respectively. Although, the decomposition of 1 at.% Eu-doped zinc titanate to ZnO and $Eu_2Ti_2O_7$ takes place, one can say that within statistical errors the doping practically does not change the activation energy of the crystallite growth.

Fig. 9 shows the DTA curves of the powders with varied europium concentrations pre-treated in air and measured at different heating rates. A broad exothermic peak appears on the DTA curves around 560 °C that corresponds to the crystallization peaks of zinc titanate. From Fig. 9 it is evident that the peak temperature T_P shifts to higher temperatures with increasing heating rate. By increasing the concentration of europium in the samples the peak temperature also shifts to higher temperatures and the crystallization is slightly suppressed. To evaluate the activation energy of crystallization processes three different approximations represented by Ozawa equation – Eq. (4) [21], Kissinger equation – Eq. (5) [22] and Augis–Bennett equation – Eq. (6) [23], respectively, were taken into account:

$$\ln(\beta) = -\frac{E_A}{R \cdot T_P} + A \tag{4}$$

$$\ln\left(\frac{\beta}{T_P^2}\right) = -\frac{E_A}{R \cdot T_P} + A \tag{5}$$

$$\ln\left(\frac{\beta}{T_P - T_0}\right) = -\frac{E_A}{R \cdot T_P} + A \tag{6}$$

In Eqs. (4)–(6), β represents the heating rate, T_P is the peak temperature at the exothermal peak, T_0 is equal to 273.15 K and represents the conversion to Celsius scale, E_A is the activation energy of the crystallization of the amorphous phase, R is the ideal gas constant and A is the integration constant. Calculated values of the terms on the left side of Eqs. (4)–(6) plotted versus the reciprocal peak temperature and their corresponding linear fits are shown in Figs. 10 and 11 for undoped and 0.5 at.% Eu-doped zinc titanate, respectively. With respect to the peak temperature T_P all curves representing doped samples are shifted to lower values of T_P^{-1}. The activation energies determined from the linear fits are summarized in Table 2. They can be interpreted as energy required to transport molecular segments to the crystallization surface [24]. All three methods give similar results for the particular samples.

3.4. Reaction mechanisms

To clarify crystallization processes, the DTA peaks were further analyzed and Avrami parameters were calculated from the Johnson–Mehl–Avrami equation expressed in the Ozawa's modi-

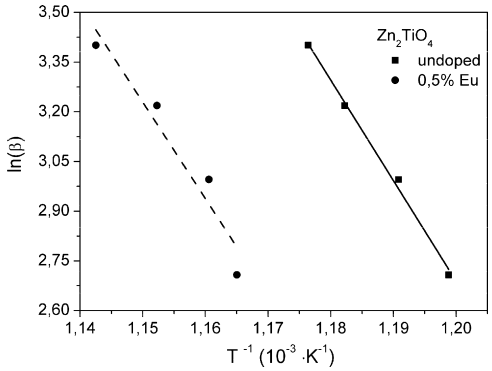

Fig. 10. Plots of the Ozawa equation for experimental data determined with the undoped and 0.5 at.% Eu-doped Zn_2TiO_4.

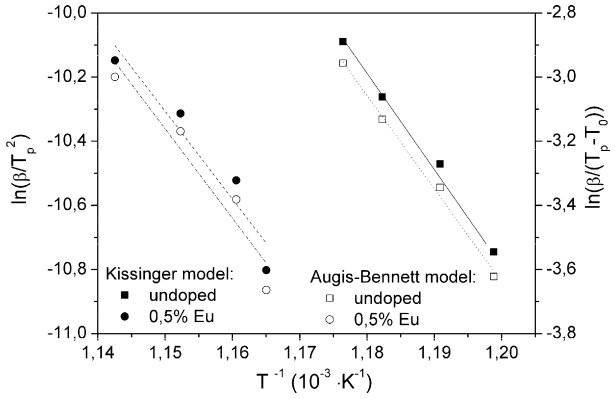

Fig. 11. Plots of Kissinger (left scale) and Augis–Bennett (right scale) equations for the undoped and 0.5 at.% Eu-doped Zn_2TiO_4.

fication for linear heating rates – Eq. (7) [25]:

$$-n = \left.\frac{d\{\log[-\ln(1-\alpha)]\}}{d\log\beta}\right|_T, \quad (7)$$

where n represent the Avrami parameter obtained from the slope of the plot $\log[-\ln(1-\alpha)]$ versus $\log\beta$, α is the volume fraction crystallized at time t and β is the heating rate. The value of α was calculated for all fixed temperatures as the ratio of the partial integration area of the crystallization peak at the selected temperature T over the total integration area of the crystallization peak.

The results in Fig. 12 show that in the case of Zn_2TiO_4 large values of n parameter rapidly decrease with the increased heat-treatment temperature to values calculated for the RE-doped samples. The high values of n at the beginning of the crystallization of Zn_2TiO_4 are typical for the homogeneous nucleation with the three-dimensional growth at the constant nucleation rate [25]. Once uniform nanocrystals are formed filling the volume of the initial material, the crystallization mechanism is changed and the cellular recrystallization takes place. As a result nanocrystals regularly grow together as one can see from Fig. 5a and c; this growth

Table 2
Activation energy of crystallization calculated for particular samples using different approximations.

Dopant	Kissinger approximation (kJ/mol)	Augis–Bennett approximation (kJ/mol)	Ozawa approximation (kJ/mol)
Undoped Zn_2TiO_4	250 ± 19	242 ± 12	252 ± 12
0.5 at.% Eu	228 ± 46	232 ± 46	242 ± 21
0.5 at.%Tm	212 ± 47	216 ± 47	227 ± 47
0.5 at.% Er	191 ± 25	195 ± 25	205 ± 25

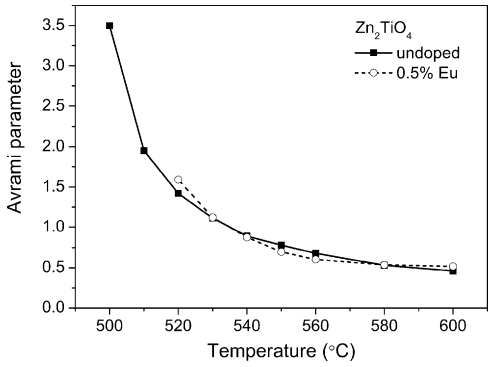

Fig. 12. Calculated Avrami parameters for undoped and 0.5 at.% Eu-doped Zn_2TiO_4.

is limited by the diffusion through the crystal boundary and n parameters are accordingly decreased. Despite the lower crystallization energies calculated for RE elements doped samples, the crystallization is shifted to higher heat-treatment temperatures. The calculated values of the Avrami parameters are typical for the site saturated nucleation followed by the three dimensional grow controlled by the diffusion which rapidly pass into the cellular recrystallization [25]. Such phenomena can be explained by the incorporation of RE ions into the pre-formed Zn_2TiO_4 clusters. As shown above RE ions particularly substitute zinc ions inside the zinc titanate structure forming nucleation centers for generated zinc titanate and block the crystallite grow till they are fully incorporated into the crystalline lattice. Once RE elements are integrated inside the crystalline lattice the crystallization is facilitated that is characterized by the calculated activation energies of crystallization. Thus, the formation of smaller uniform crystallites is more favorable in the case of doped zinc titanates. On the other hand the crystallite growth is more favorable in the case of undoped zinc titanate. These effects are explicitly remarkable for the samples heat-treated to 1000 °C in which Zn_2TiO_4 grown up nearly to micrometric grains and the Eu doped zinc titanate still remained in the form of nanocrystalline powder as one can clearly see in the SEM pictures Fig. 5c and d.

4. Conclusions

By using the sol–gel method thermally stable undoped, as well as europium, erbium and thulium-doped zinc titanates have successfully been prepared. The solubility of these rare earth elements in Zn_2TiO_4 matrix has been found to be limited approximately to 0.5 at.%. A new crystalline phase of RE pyrochlorates has been observed for RE concentrations higher than this limit. Activation energies of crystallization processes and activation energies of crystallites growth were calculated on the base of XRD and DSC analysis. From the calculated Avrami parameters it has been found that in the case of undoped Zn_2TiO_4 the crystallization process has the character of homogenous nucleation followed by the three dimensional growth at a constant nucleation rate which finally pass into the cellular recrystallization controlled by the diffusion of matter. Although the activation energy of the crystal growth is not significantly affected by the presence of RE ions and side-formed pyrochlorates, introduced RE ions substitute zinc ions in the crystalline matrix of Zn_2TiO_4 forming thus nucleation centers. Consequently, the crystallization process has the character of the site saturated nucleation followed by the three dimensional growth and cellular recrystallization and resulting in the formation of smaller and more uniform nanocrystals in comparison with the undoped Zn_2TiO_4.

Acknowledgements

The authors acknowledge for the financial support from the Czech Science Foundation under contract no. 102/10/2139. The authors thank Z. Jarchovsky from the Institute of Photonics and Electronics AS CR, Prague for SEM analysis.

References

[1] S.F. Bartram, R.A. Slepetys, Journal of the American Ceramic Society 44 (10) (1961) 493–499.
[2] M. Pineda, et al., Applied Surface Science 119 (1–2) (1997) 1–10.
[3] Z.X. Chen, et al., Journal of Catalysis 161 (2) (1996) 730–741.
[4] S.C. Souza, et al., Journal of Thermal Analysis and Calorimetry 79 (2) (2005) 451–454.
[5] H.T. Kim, et al., Journal of the American Ceramic Society 84 (5) (2001) 1081–1086.
[6] C.F. Shih, et al., Journal of Alloys and Compounds 485 (1–2) (2009) 408–412.
[7] C. Ye, et al., Applied Physics A: Materials Science & Processing 90 (2) (2008) 375–378.
[8] S.A. Mayén-Hernández, et al., Journal of Materials Science: Materials in Electronics 18 (11) (2007) 1127–1130.
[9] A.C. Chaves, et al., Journal of Solid State Chemistry 179 (4) (2006) 985–992.
[10] J. Mrazek, et al., Journal of Physical Chemistry C 114 (7) (2010) 2843–2852.
[11] P.F.S. Pereira, et al., Journal of Luminescence 126 (2) (2007) 378–382.
[12] C.-C. Yang, S.-Y. Chen, S.-Y. Cheng, Powder Technology 148 (1) (2004) 3–6.
[13] J.I. Langford, A.J.C. Wilson, Journal of Applied Crystallography 11 (April) (1978) 102–113.
[14] T. Ishioka, et al., Spectrochimica Acta Part A—Molecular and Biomolecular Spectroscopy 54 (12) (1998) 1811–1818.
[15] G. Starukh, et al., Zeitschrift Fur Physikalische Chemie—International Journal of Research in Physical Chemistry & Chemical Physics 221 (3) (2007) 349–360.
[16] F.X. Perrin, V. Nguyen, J.L. Vernet, Journal of Sol–Gel Science and Technology 28 (2) (2003) 205–215.
[17] J. Preudhom, P. Tarte, Spectrochimica Acta Part A—Molecular Spectroscopy 27 (6) (1971) 845.
[18] J. Preudhom, P. Tarte, Spectrochimica Acta Part A—Molecular Spectroscopy 27 (7) (1971) 961.
[19] Y.L. Chai, et al., Materials Research Bulletin 43 (5) (2008) 1066–1073.
[20] Y.S. Chang, et al., Journal of Crystal Growth 243 (2) (2002) 319–326.
[21] T. Ozawa, Bulletin of the Chemical Society of Japan 38 (11) (1965) 1881.
[22] J. Llopiz, et al., Thermochimica Acta 256 (2) (1995) 205–211.
[23] J.A. Augis, J.E. Bennett, Journal of Thermal Analysis 13 (2) (1978) 283–292.
[24] N. Bayri, et al., Journal of Non-Crystalline Solids 355 (1) (2009) 12–16.
[25] J. Malek, T. Mitsuhashi, Journal of the American Ceramic Society 83 (8) (2000) 2103–2105.